Structural, magnetic, and electrical properties of single-crystalline $La_{1-x}Sr_xMnO_3$ $(0.4<x<0.85)$

J. Hemberger,[1] A. Krimmel,[1] T. Kurz,[1] H.-A. Krug von Nidda,[1] V. Yu. Ivanov,[2] A. A. Mukhin,[2] A. M. Balbashov,[3] and A. Loidl[1]

[1]*Experimentalphysik V, Elektronische Korrelationen und Magnetismus, Institut für Physik, Universität Augsburg, D-86135 Augsburg, Germany*

[2]*General Physics Institute of the Russian Academy of Sciences, 38 Vavilov Street, 117942 Moscow, Russia*

[3]*Moscow Power Engineering Institute, 14 Krasnokazarmennaya Street, 105835 Moscow, Russia*

(Received 14 December 2001; revised manuscript received 11 April 2002; published 11 September 2002)

We report on structural, magnetic, and electrical properties of Sr-doped $LaMnO_3$ single crystals for doping levels $0.4\leqslant x\leqslant 0.85$. The complex structural and magnetic phase diagram can only be explained assuming significant contributions from the orbital degrees of freedom. Close to $x=0.6$ a ferromagnetic metal is followed by an antiferromagnetic metallic phase below 200 K. This antiferromagnetic metallic phase exists in a monoclinic crystallographic structure. Following theoretical predictions this metallic antiferromagnet is expected to reveal an $(x^2\text{-}y^2)$-type orbital order. For higher Sr concentrations an antiferromagnetic insulator is established below room temperature.

DOI: 10.1103/PhysRevB.66.094410 PACS number(s): 71.30.+h, 72.80.Ga

I. INTRODUCTION

The fascinating phase diagrams of the doped maganites result from a subtle interplay of spin, charge, orbital, and lattice degrees of freedom. In $La_{1-x}Sr_xMnO_3$ the main body of experimental investigations has been carried out for Sr concentrations $x<0.5$. This partly has been due to the fact that colossal magnetoresistance effects[1] show up around $x=0.3$, which in the beginning of the research seemed to be rather promising for application. On the other hand, single crystals for $x>0.5$ are hard to grow and hence, only rarely have been investigated.

Already at low concentrations ($x<0.5$) a rather complex phase diagram evolves, which is due to the fact that in addition to superexchange (SE) and double-exchange (DE) interactions, charge order (CO) and structural effects via orbital ordering are of outstanding importance. For $x<0.2$, a long-range cooperative Jahn-Teller (JT) effect establishes orbital order (OO), which finally determines the antiferromagnetic (AFM) spin state of A type in the pure compound at low temperatures. With increasing Sr doping ($x<0.1$) a ferromagnetic (FM) component evolves in addition to the AFM order of subsequent planes, which is explained in terms of electronic phase separation[2] or, following the time-honored ideas of de Gennes,[3] in terms of a canted AFM (CA) state. However, within this model of competing SE and DE interactions clearly the importance of lattice distortions has to be taken into account.[4] On further increasing x $(0.1\leqslant x\leqslant 0.17)$, it seems clear that a new type of orbital order, probably connected with CO, determines the low-temperature insulating ferromagnet (FM) around $x=0.125$.[5–7] Finally, for Sr concentrations $x>0.17$, the long-range JT distortions become suppressed and a ferromagnetic metal evolves below the FM phase transition, which is stable almost up to half filling.

After the early work on La:$SrMnO_3$, which is summarized by Goodenough and Longo,[8] the complex phase diagram has been studied by many groups and a more or less coherent picture can be deduced from the variety of experimental results reported.[6,9–12] From the systems with narrower bandwidth (e.g., $L_{1-x}A_xMnO_3$ with $L=$Nd, Pr, Sm and $A=$Ca, Sr[13,14]) an extreme asymmetry between the hole- and electron-doped regimes is well known and it seems highly interesting also to investigate the electron doped $La_{1-x}Sr_xMnO_3$. However, for $x>0.5$ much less experimental information is available.

Structural, resistivity, and magnetization results for $x=0.5$ and 0.54 were reported by Akimoto *et al.*[15] For $x=0.54$, they reported an orthorhombic ($Pbnm$) nuclear and an A-type AFM structure at 10 K. Results for similar Sr concentrations $0.5<x<0.6$ were published by Moritomo *et al.*[16] On increasing x, the crystal symmetry changes from rhombohedral ($R3c$) to pseudotetragonal at $x=0.54$ with $a\approx b<c/\sqrt{2}$. For concentrations around $x=0.55$, a metallic AFM phase, with A-type spin structure at low temperatures, is followed by a FM metallic (M) state at elevated temperatures.[16] Polycrystalline $La_{1-x}Sr_xMnO_3$ has been investigated by Fujishiro *et al.*[17] by magnetization, electrical resistivity, and ultrasonic techniques. They arrive at a different phase diagram, with an insulating (I) state for all concentrations $x>0.5$. Similar findings were reported by Patil *et al.*,[18] who also investigated ceramic samples for $0.46\leqslant x\leqslant 0.53$. They found a sequence of magnetic and charge-order transitions and interpreted their results in terms of electronic phase separation.

Further interest in the overdoped manganites arises from the fact that for the insulating regions of the phase diagram electronic phase separation in form of stripes[20] or bistripes[21] has been reported. This special form of CO certainly is driven by OO.[22] Also, theoretically the phase diagrams of the doped manganites have been investigated in great detail.[2,13,22–24] Specifically in Ref. 24, the overdoped regime was investigated using DE within degenerate orbitals. Depending on the bandwidth, on increasing electron doping a sequence of spin structures of type A, C, A, and FM has been predicted.[24,25]

In order to clarify the situation and to shed some light on the complex and complete (x,T) phase diagram in $La_{1-x}Sr_xMnO_3$, we grew a series of single crystals for concentrations $(0.4<x<0.85)$. We were not able to grow crystals with higher Sr concentrations. The reason seems to be rather clear as $SrMnO_3$ reveals a hexagonal crystal structure and obviously there exists a miscibility gap for concentrations close to pure $SrMnO_3$. In the following, we present detailed structural, magnetic susceptibility, magnetization, and electrical resistivity results for the complete series of crystals. From the results we construct a detailed phase diagram. Polycrystalline $SrMnO_3$ has been investigated to complete the phase diagram. These experiments are a continuation of earlier work on crystals with low Sr-doping levels, which has been published previously[6] and has been included to present the complete (x,T) phase diagram of $La_{1-x}Sr_xMnO_3$ for $0\leqslant x\leqslant 1$.

II. EXPERIMENTAL DETAILS

$La_{1-x}Sr_xMnO_3$ single crystals were grown by a floating-zone method with radiation heating similar to the techniques as described in Ref. 26. For these crystals with Sr concentrations $x\geqslant 0.5$, different atmospheric conditions ranging from air atmosphere to excess oxygen pressure up to 50 atm were tested to optimize the growth process. Nevertheless an uncertainty in the control of the concentration x of up to 2% cannot be ruled out. To complement the phase diagram pure $SrMnO_3$ has been grown using standard ceramic techniques. Powder x-ray-diffraction measurements were performed utilizing Cu-K_α radiation with $\lambda = 0.1541$ nm.

The magnetic susceptibility and magnetization were measured using a commercial superconducting quantum interference device magnetometer ($1.5<T<400$ K, $H\leqslant 50$ kOe) and an ac magnetometer that operates up to magnetic fields of $H=140$ kOe. The electrical resistance has been measured using standard four-probe techniques in home-built cryostats and ovens from 1.5 K to 600 K.

III. RESULTS AND DISCUSSION

A. X-ray diffraction

To demonstrate the quality of the single crystals under investigation, we powdered pieces of the single crystals used for magnetic and transport measurements and performed detailed Rietveld refinements of the diffraction profiles for samples with Sr concentrations $0.55\leqslant x\leqslant 0.85$ at room temperature. Figure 1 shows the diffraction profiles, the refinement and the difference pattern for $x=0.55$ (upper panel) and $x=0.75$ (lower panel). First of all, we want to stress that all reflections can be indexed and no impurity phases are apparent above the background level, even no spurious amount of $SrMnO_3$ which has been reported in all previous investigations.[8,15–17] At first sight one recognizes that with increasing Sr concentration x the crystals almost approach cubic symmetry, which is expected for concentrations with a tolerance factor close to 1. This is demonstrated by the insets in Fig. 1, showing the splitting of the [220]/[004] reflections that provides direct experimental evidence of the c/a ratio

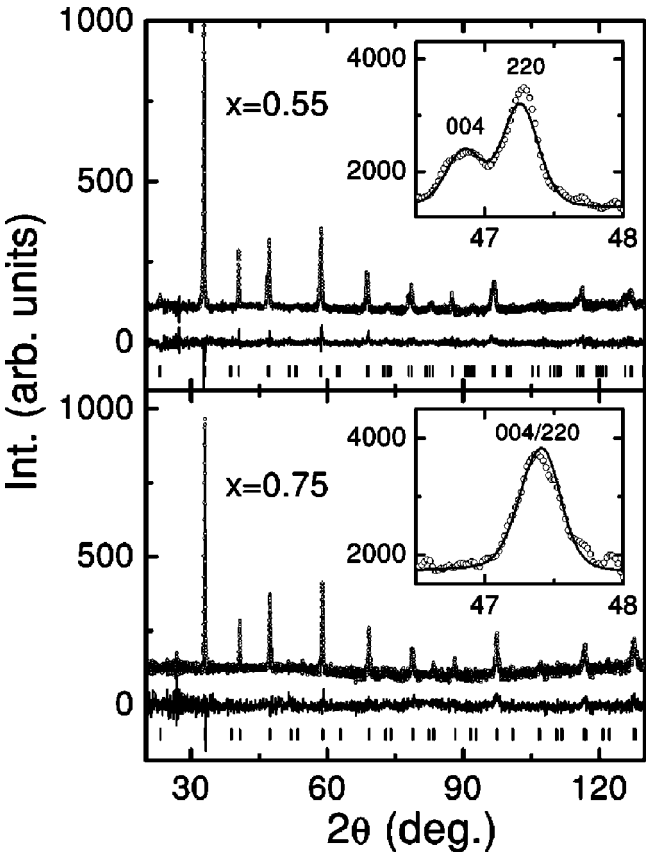

FIG. 1. X-ray-diffraction profiles of $La_{1-x}Sr_xMnO_3$ for concentrations $x=0.55$ (upper frame) and $x=0.75$ (lower frame). The solid lines correspond to the results of a Rietveld refinement. The difference patterns are indicated in each frame. The insets show the splitting of the [220] and [004] reflections, denoting the decrease of the tetragonal distortion with increasing x.

and hence on the tetragonal distortion. For $x=0.55$, a clear splitting of the reflections can be detected, while for $x=0.75$ no apparent splitting is visible and a splitting can only be derived via the broadening of the reflections in a detailed Rietveld refinement with well-defined resolution parameters. Hence the samples near $x=0.8$ are very close to cubic symmetry.

From the Rietfeld refinement we determined the lattice constants of the samples under investigation. The results are listed in Table I. At room temperature the structure changes from rhombohedral (R) at $x=0.5$ to tetragonal (T) at $x=0.55$ and finally to hexagonal (H) close to pure $SrMnO_3$. We would like to recall that $SrMnO_3$ was only prepared in ceramic form and we were not able to grow crystals beyond strontium concentrations $x=0.85$. The room-temperature tetragonal phase extends over a broad concentration range, with a significant change of the tetragonal distortion. For $x=0.55$, we find a value of $c/\sqrt{2}a\approx 1.01$. Note that for this concentration ferromagnetism is established already at room temperature. On increasing x this ratio is reduced yielding values close to 1, however now in the paramagnetic phase, but still on the verge of magnetic order. It is clear that the c/a ratio will strongly depend on the orbital structure, i.e., whether the orbitals are aligned as $d_{x^2-y^2}$ or as $d_{3z^2-r^2}$.

TABLE I. Room-temperature crystal symmetry and lattice parameters of $La_{1-x}Sr_xMnO_3$ for Sr concentrations ($0.5 \leqslant x \leqslant 1.0$). The diffraction data for $x<1$ were derived from single crystalline material that was powdered for the diffraction measurements. The two lowest rows display Curie-Weiss temperatures T_{CW} and the effective paramagnetic moments μ_{eff} obtained from the linear regime of the inverse susceptibility below $T=400$ K.

x	0.5	0.55	0.6	0.65	0.75	0.85	1.0
Crystal Structure	rhombohedral	tetragonal	tetragonal	tetragonal	tetragonal	tetragonal	hexagonal
a (Å)	5.461	5.438	5.448	5.437	5.419	5.404	5.452
c (Å)		7.753	7.672	7.670	7.686	7.665	9.084
$c/\sqrt{2}a$		1.008	0.996	0.997	1.002	1.003	
α (deg)	60.16						
T_{CW} (K)	333	313	299	255	64	−2	−980
μ_{eff} (μ_B)	5.1	5.0	4.9	4.8	4.9	4.6	4.0

However, systematic temperature-dependent x-ray-diffraction measurements are needed to arrive at final conclusions. From preliminary temperature-dependent x-ray-diffraction experiments (down to 80 K), we found that for $0.5<x<0.7$ the symmetry is lowered and the structure changes into a monoclinic (Mc) phase characterized by space group $P2_1/m$. Figure 2 illustrates the evolution of superlattice reflections for $x=0.6$ due to the monoclinic distortion on cooling. At the boundaries of this monoclinic low-temperature phase for $x \approx 0.5$ and $x \approx 0.7$, we suggest that the system enters into a structurally mixed phase where the Mc phase coexists with a R and T phase, respectively. However, a more detailed evaluation is necessary to analyze these two-phase regions. A detailed report on the structural properties will be given elsewhere.[27] It should be noticed that a low-temperature monoclinic phase with space group $P2_1/m$ has been established in the doped manganites $La_{0.5}Ca_{0.5}MnO_3$ and $Pr_{0.6}(Ca_{1-x}Sr_x)_{0.4}MnO_3$, as well as in $Pr_{0.5}Sr_{0.5}MnO_3$.[28–30] Furthermore, the presence of monoclinic domains within an orthorombic matrix has been reported for $Pr_{0.7}Ca_{0.25}Sr_{0.05}MnO_3$ and $Pr_{0.75}Sr_{0.25}MnO_3$ on the basis of high-resolution microscopy.[31]

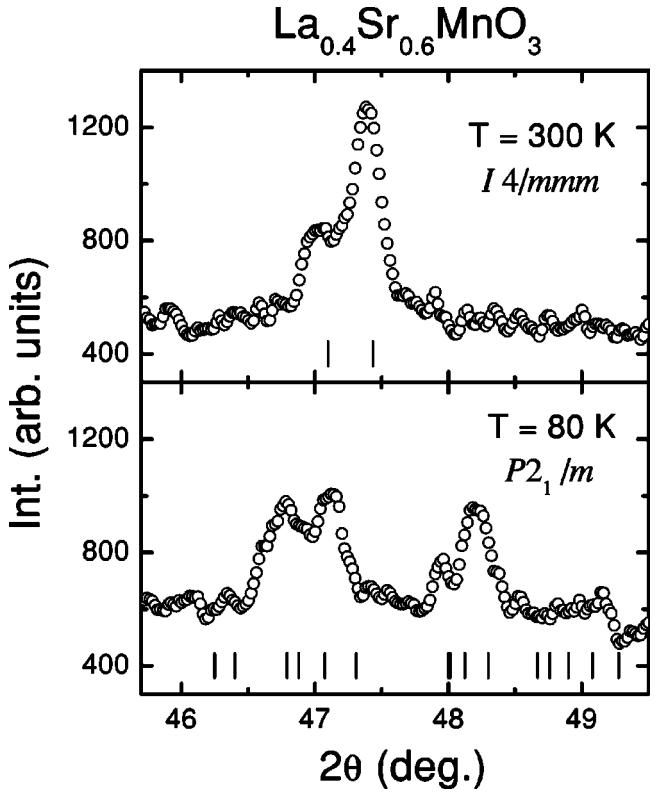

FIG. 2. Parts of the temperature-dependent x-ray powder-diffraction patterns of $La_{0.4}Sr_{0.6}MnO_3$ for $46° < 2\Theta < 49°$. At $T=80$ K pronounced superlattice reflections around $2\Theta \approx 48°$ indicate a monoclinic distortion.

B. Transport properties

Figure 3 shows the temperature dependence of the electrical resistivity below room temperature. Clearly, $La_{1-x}Sr_xMnO_3$ reveals a metallic conductivity for $0.4<x<0.6$. These findings differ from those reported by Patil *et al.*[18] for concentrations close to $x=0.5$ obtained from ceramic samples, where the resistivity increases towards low temperatures. From optical measurements these authors find indications for an anisotropy of the conductivity. This fact together with possible grain effects in ceramic samples could explain the different results.

For Sr concentrations $x=0.625$ and 0.7, a significant increase of the resistivity occurs below 250 K. Finally, in the samples with $x>0.7$ this feature is sharper and denotes the transition from the paramagnetic to the antiferromagnetic state. Towards low temperatures a purely semiconducting behavior can be found. It seems that the samples with Sr concentration $x \approx 0.7$ belong to a two-phase region separating metallic and insulating regimes. At the same time the system is close to a phase boundary between the monoclinic and tetragonal crystal structures. Nevertheless, the sample with $x=0.7$ remains a candidate for the occurrence of electronic phase separation for $T<200$ K. To investigate also the high-temperature electronic behavior, we measured the electrical resistance for some representative samples up to 600 K. The results for $x=0.5$ and 0.75 are shown in the inset. For $x=0.5$, the metallic behavior at low temperatures changes into the temperature characteristics of a bad metal at elevated temperatures. For $x>0.7$ a bad metallic behavior for $T>250$ K changes into strongly semiconducting temperature

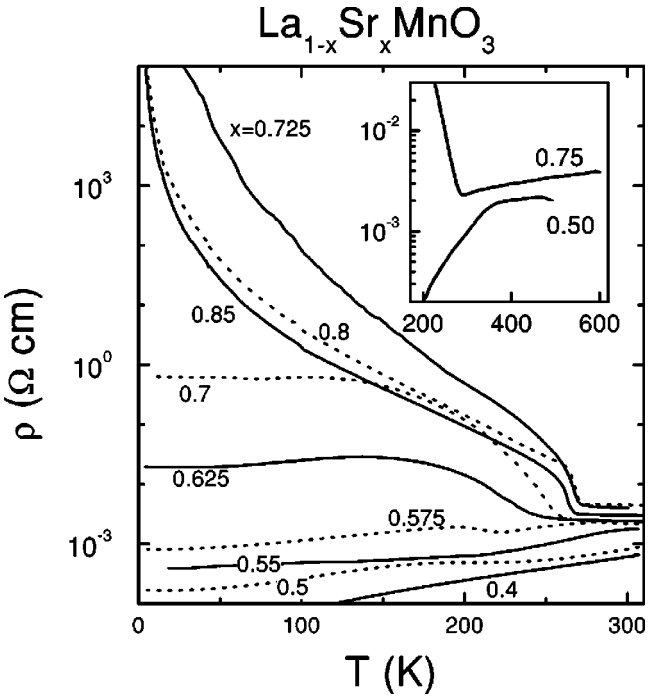

FIG. 3. Temperature dependence of the resistivity in $La_{1-x}Sr_xMnO_3$ for different concentrations $0.4 \leqslant x \leqslant 0.85$ as indicated in the figure. The inset shows the resistivity for $x = 0.5$ and $x = 0.75$ measured also at higher temperatures.

characteristics below. The low-temperature resistivity as a function of Sr concentration exhibits a maximum around $x \approx 0.75$. This may indicate a CO state at electronic quarter filling of the e_g bands.

C. Magnetization and magnetic susceptibility

The magnetic dc susceptibility (M/H measured at 1 kOe) of $La_{1-x}Sr_xMnO_3$ is shown in Fig. 4 in the upper frame. For $x = 0.4$ at 370 K, we find the pure ferromagnetic phase transition that is driven by DE interactions and is characteristic for the materials showing a colossal magnetoresistance (CMR) effect. For $x = 0.5$ and 0.6, the magnetization decreases below 250 K indicating that the ferromagnetic moments become reduced at low temperatures. This may be due to a slight canting of the spins or due to electronic phase-separation effects. Similar findings for $0.46 \leqslant x \leqslant 0.53$ were interpreted in terms of phase separation within a charge-ordered state.[18] We would like to recall that for $x \approx 0.5$ we found indications of a two-phase region of a rhombohedral and a monoclinic structure. At the moment it is unclear, whether this is a structural two-phase region, or whether the ground state can be explained in terms of electronic phase separation between FM and AFM regions including scenarios such as stripe or bistripe formation.

Well-defined cusps appear for $x = 0.65$ and 0.7, which indicate the vanishing of a spontaneous ferromagnetic moment and the presence of a nearly completely antiferromagnetic (AFM) spin structure at low temperatures. It is important to note that we observed a pronounced temperature hysteresis at these cusps typical for a first-order magnetic transition. Finally for $x > 0.7$, the characteristics of purely antiferromagnetic phase transitions are detected. From the inverse susceptibilities, which are shown in the lower frame of Fig. 4, we can deduce the Curie-Weiss (CW) temperatures that continuously decrease while the Sr concentration increases from $x = 0.4$ to $x = 0.7$ (cf. Table I). Beyond this concentration a significant decrease of the CW temperatures appears and finally, for $x = 0.85$, a negative CW temperature can be read off. For the concentrations $0.55 \leqslant x \leqslant 0.7$ in addition a distinct deviation from the CW behavior can be detected well above the magnetic ordering temperature indicating the presence of strong spin fluctuations or even of short-range magnetic order.

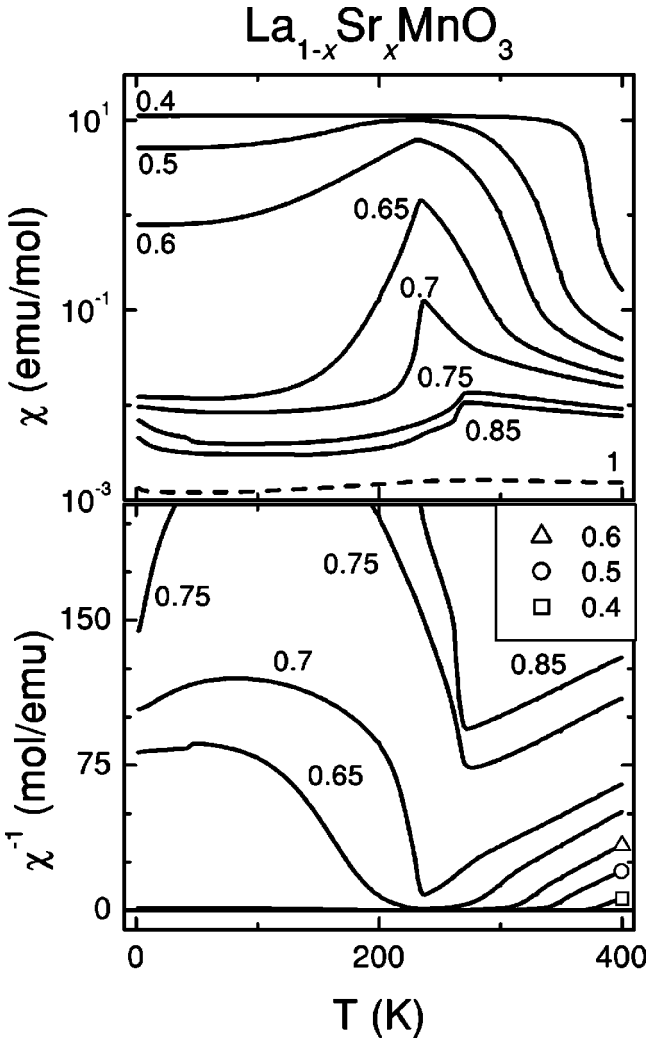

FIG. 4. Temperature dependence of the magnetic susceptibility in $La_{1-x}Sr_xMnO_3$ as measured at a dc magnetic field of 1 kOe for Sr concentrations from 0.4 to 0.85. In the upper frame the susceptibility is shown as a function of temperature. The lower frame shows the inverse susceptibilities vs T.

To further elucidate the low-temperature magnetic properties of $La_{1-x}Sr_xMnO_3$, Fig. 5 shows the magnetization at 5 K for a series of crystals with concentrations $0.5 < x < 0.65$. An almost pure antiferromagnet at $x = 0.65$ is followed by an increasing ferromagnetic component on decreasing x. But even at $x = 0.5$ only two-third of the full possible ferromag-

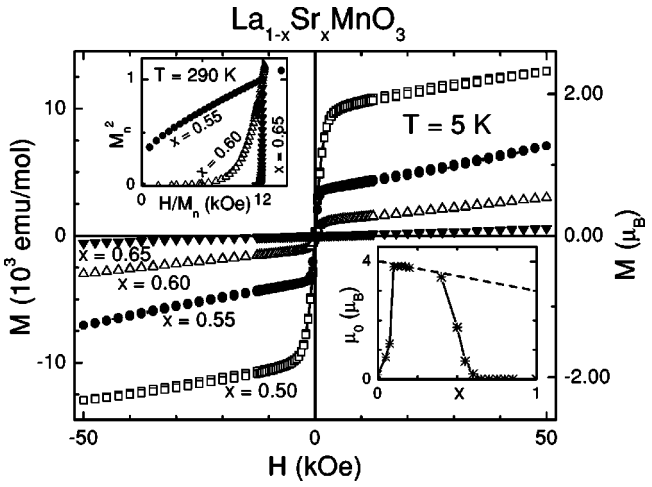

FIG. 5. Low-temperature ($T=5$ K) magnetization of $La_{1-x}Sr_xMnO_3$ as a function of magnetic field for concentrations $x=0.5$, 0.55, 0.6, and 0.65. The lower right inset shows the remnant (ferromagnetic) saturated moment as a function of concentration. The dashed line indicates the saturated moment assuming that all Mn ions (Mn^{3+} and Mn^{4+}) contribute only with their spin values to the ordered moment. The upper left inset shows the normalized magnetization at 290 K for concentrations $x=0.5$, 0.55, and 0.6 presented as M_n^2 vs H/M_n with $M_n=M/M(12\ \text{kOe})$.

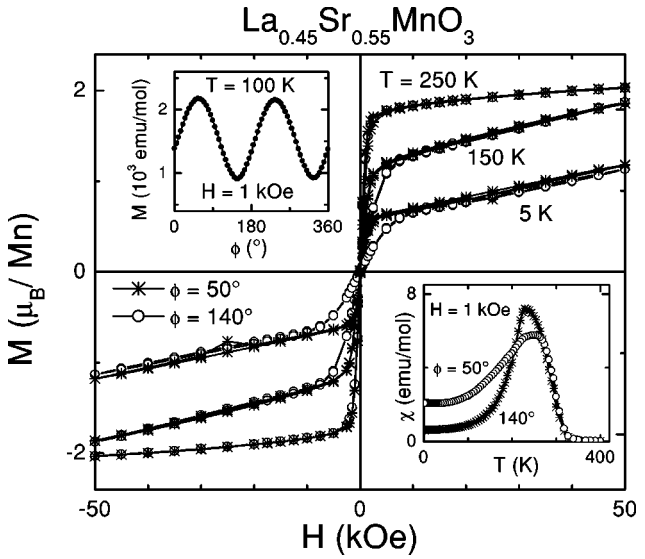

FIG. 6. Magnetization as a function of external field in $La_{0.45}Sr_{0.55}MnO_3$ measured at different temperatures and different orientations with respect to the external field (see upper inset). The solid lines are drawn to guide the eye. The lower inset displays the temperature dependence of the magnetic dc susceptibility $\chi=M/H$, measured at these different orientations.

netic magnetization is observed at low fields and on increasing external field the magnetization increases strictly linearly, which can be explained in terms of a canted antiferromagnet, whose canting angle becomes reduced in increasing fields, or in terms of electronic phase separation. Including earlier published results,[6] the lower inset of Fig. 5 demonstrates how the ferromagnetic moment evolves in the complete concentration regime. The expected spin-only FM moment only evolves for Sr concentrations $0.2<x<0.4$ and approaches values close to zero for lower and higher Sr concentrations. The upper inset of Fig. 5 compares the field dependence of the magnetization for the concentrations $x=0.55$, 0.6, and 0.65 at $T=290$ K. The representation M_n^2 vs H/M_n (Arrot[19] plot) demonstrates the presence of a spontaneous FM component (i.e., finite M^2 at $H=0$) for $x=0.55$. At the same temperature the behavior of $x=0.65$ is purely paramagnetic (i.e., H/M is constant). The curve for $x=0.6$ exhibits an intermediate behavior, denoting the presence of strong FM fluctuations or short-range (SR) order. This corresponds to the strong deviations from the Curie-Weiss behavior discussed earlier (see Fig. 4).

In what follows, we wanted to study the magnetic anisotropy close to half filling in more detail. Around $x=0.55$, the ferromagnetic phase at elevated temperatures is followed by a further magnetic phase transition that significantly reduces the magnetization (see Fig. 4). To elucidate the temperature evolution of this weak ferromagnetic regime in more detail, Fig. 6 shows the magnetization vs external field in $La_{0.45}Sr_{0.55}MnO_3$ for a series of temperatures. At 250 K, just below the FM phase transition a strong ferromagnetic hysteresis evolves and, taking into account the elevated temperature, almost the full saturated moment of Mn^{3+}/Mn^{4+} can be detected. However, below 200 K the magnetization at moderate fields becomes significantly reduced and reveals a strictly linear increase of M as function of field. Finally at 5 K the FM component amounts approximately 0.5 μ_B only.

To study the anisotropy of this magnetic ground state, the data were taken for two different orientations of the sample with respect to the external field. The upper inset of Fig. 6 shows the angular dependence of the magnetization as observed at $T=100$ K when the sample was rotated around an axis approximately within the a-b plane. From this a hard and an easy axis were defined, which differ by almost a factor of 2.5 in the magnetization values. The lower inset of Fig. 6 shows the temperature dependence of the magnetic susceptibility measured for these both orientations. The distinct evolution of anisotropic behavior below $T\approx 250$ K can be observed. This behavior clearly is different from the anisotropy observed for strontium concentrations of $x=0.05$, where the magnetization is zero along a and b and finite along c, indicating a slight canting of the moments out of the a-b plane.[6] It seems that for $x=0.55$ the AFM structure at low temperatures is certainly more complex. Nevertheless, it has to be stated, that neither a considerable uncertainty concerning the determination of the a-b plane nor possible twinning of the sample can be ruled out. However, as observed for $x=0.05$ (Ref. 6) the paramagnetic susceptibility again is fully isotropic for temperatures above the magnetically ordered regime. It is interesting to note that the anisotropy changes in the (canted) antiferromagnetic state. These results indicate either a canted spin structure or phase separation assuming ferromagnetic clusters within an antiferromagnetic matrix. But, of course, we cannot exclude more complex phase-separation scenarios.[20,21] It also should be kept in mind that the sample under consideration still behaves metallic in the paramagnetic (PM), in the FM, and in the canted AFM state, respectively.

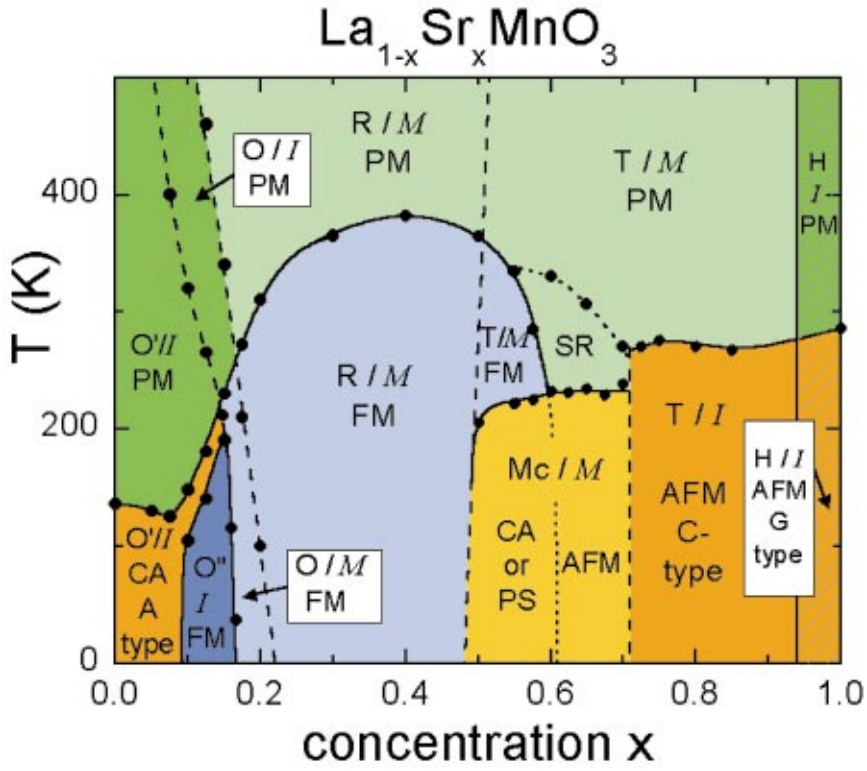

FIG. 7. (Color) Phase diagram of $La_{1-x}Sr_xMnO_3$ for the complete concentration regime, including results of Ref. 6. The crystal structures (Jahn-Teller distorted orthorhombic: O′, orthorhombic O; orbital-ordered orthorhombic: O″, rhombohedral: R, tetragonal: T, monoclinic: Mc, and hexagonal: H) are indicated as well as the magnetic structures [paramagnetic: PM (green), short-range order (SR), canted (CA), *A*-type antiferromagnetic structure: AFM (yellow), ferromagnetic: FM (blue), phase separated (PS), and AFM *C*-type structure] and the electronic state [insulating: *I* (dark), metallic: *M* (light)].

D. Phase diagram

Finally, in Fig. 7 we present the phase diagram for the complete concentration regime $0 \leqslant x \leqslant 0.85$, where mixed single crystals can be grown. We included the results from earlier work ($0 \leqslant x \leqslant 0.3$).[6] The complex sequence of magnetic phases at low concentrations is highly influenced by the cooperative JT distortion of the O′ phase and by the orbital order of the O″ phase.[5] For $x > 0.2$ a large ferromagnetic regime evolves which reveals a rhombohedral structure and shows CMR effects throughout. For $x > 0.5$, a tetragonal phase appears which is a FM metal. On decreasing temperature it undergoes a transition into a monoclinic antiferromagnetic state, but still exhibits metallic behavior. We would like to recall that in $Pr_{0.5}Sr_{0.5}MnO_3$ and $Nd_{0.5}Sr_{0.5}MnO_3$ the FM and *M* phase is followed by an insulating AFM phase that reveals a *CE*-type spin structure for the Nd and an *A*-type layered spin structure for the Pr compound.[30] The latter shows no clear signs of CO.[30] However, for $Nd_{0.45}Sr_{0.55}MnO_3$ a metallic behavior has been detected within the ferromagnetic layers, while the resistivity along *c* revealed a semiconducting characteristic.[32] It seems that in the La:Sr series of the manganites this two-dimensional metallic phase, which is antiferromagnetic, evolves for $x \approx 0.6$. There the resistivity remains fully metallic ($d\rho/dT > 0$) for all temperatures (see Fig. 3) and at $T = 5$ K only a weak ferromagnetic moment can be detected (Fig. 5).

This metallic and AFM state is monoclinic and is embedded into structurally different regions (R for $x < 0.5$ and T for $x > 0.7$), depicted schematically by vertical dashed lines in Fig. 7. It seems naturally to assume that this exotic phase also is characterized by a new orbital order. Close to $x = 0.5$ it seems that the *M*/FM phase coexists with the *M*/AFM phase. According to preliminary diffraction experiments indeed also the crystallographic phases coexist. We would like to recall that from observations in conventional ferromagnets a variety of domain structures can be formed in multicomponent systems including cluster or stripe formation. Whether in this case a description in terms of electronic phase separation is adequate has to be proven in detailed experiments. At present it is also unclear how the observation of stripes[20] or bistripes[21] is compatible with the observed magnetic anisotropy. For concentrations $x \approx 0.7$ metallic and insulating domains cannot be ruled out. This we conclude from the temperature dependence of the resistivity. At the moment it remains an open question, whether a T/*I*/AFM phase coexists with an Mc/*M*/AFM state or whether in this region electronic phase separation evolves out of the structurally pure phase.

A further interesting phenomenon in this concentration range is the fact that the AFM metallic phase evolves out of a ferromagnetic metal. Probably double-exchange interactions drive the ferromagnet, while superexchange interactions are responsible for the AFM state. This can only be explained, if the orbital order changes as a function of temperature.

For concentrations $x > 0.75$, a purely AFM and insulating state evolves within a nearly cubic structure. For these concentrations the tolerance factor is close to 1. For further increasing concentrations the ABO_3 perovskite structure is unstable and no mixed crystals can be grown. $SrMnO_{3-\delta}$ reveals a layered perovskite structure.

IV. CONCLUSION

What did we learn from these experiments in addition to the existing enormous amount of knowledge on the doped

manganites? To summarize, we were able to grow high-quality single crystals of $La_{1-x}Sr_xMnO_3$ for $0 \leqslant x \leqslant 0.85$ with no parasitic phases such as $SrMnO_3$. We constructed a rather complete (x,T) phase diagram (Fig. 7) that reveals the well-established asymmetry between the hole-doped ($x < 0.5$) and the electron-doped ($x > 0.5$) regime. Of course, an essential part of this asymmetry is driven by geometrical constraints via the tolerance factor that increases from $t = 0.89$ for $x = 0$ to $t = 1.01$ for $x = 1$. Hence, on increasing concentration, $La_{1-x}Sr_xMnO_3$ reveals a decreasing buckling of the MnO_6 octahedra. But partly this asymmetry also is driven by orbital degeneracy. Close to $x = 0$ strong JT distortions reveal orbital order that concomitantly determines the *A*-type spin structure. For higher Sr concentrations and in the crystals with a high symmetry at the Mn site, orbital degeneracy will play an essential role yielding completely different spin ground states.

In Fig. 7 the combined influence of the concentration dependence of the tolerance factor and the increasing importance of orbital degeneracy as x increases is documented in the sequence of structural phases: At room temperature and for $0 \leqslant x \leqslant 0.85$ we find the crystallographic phases O′ orthorhombic, O orthorhombic, rhombohedral, and tetragonal. The corresponding series of electronic ground-state properties is insulating/spin *A*-type AFM, insulating/spin FM, metallic/spin FM, metallic/spin *A*-type AFM; insulating/spin *C*-type AFM, and finally insulating/spin *G*-type for $x = 1$. So far we did not investigate the spin structures of the magnetic phases for $x \geqslant 0.4$. Theoretically, taking SE, DE, and orbital degeneracy into account the sequence of spin structures *A*-FM-*A*-*C*-*G* has been predicted.[13] We want to stress that a pure insulating AFM state appears in all phase diagrams at high doping levels and that a *G*-type antiferromagnet is stable for $x = 1$. The spin structure close to $x = 0.8$ (AFM, *C* type) has been taken in analogy to other doped manganites and to the existing literature. For this concentration regime around $x = 0.8$ evidence for charge order can be found due to the sharp increase of the resistivity at T_N, possibly in the form of stripe or bistripe structures as it has been suggested in the literature.[21] Close to $x = 0.6$, it has been proposed that the orbitals are strictly aligned within the *a*-*b* plane forcing an *A*-type spin structure.[13] $La_{0.4}Sr_{0.6}MnO_3$ reveals antiferromagnetic order with a FM component, which is of the order of 0.1 μ_B at low fields. It is this concentration regime where also two-dimensional metallic behavior is expected.

In what follows we would like to compare the phase diagram of $La_{1-x}Sr_xMnO_3$ as observed in the present investigations with published phase diagrams of other manganites and with theoretical predictions. This discussion is based on experiments covering the hole- and electron-doped regime of the phase diagram and investigating the half doped case in detail. Experimental phase diagrams are available for La:Sr,[7] La:Ca,[33] Pr:Sr,[13,14,30] Pr:Ca,[14,34] Nd:Sr,[13,30] Sm:Sr, and Sm:Ca (Ref. 14) manganite. From these results a generic electronic phase diagram can be deduced, which yields the sequence of AFM (*A* type)/*I*, FM/*I*, FM/*M*, and AFM/*I* (*C* type). The latter spin structure dominates a broad region in the electron-doped ($x > 0.5$) crystals. It is clear that these spin structures and electronic properties are closely linked with the orbital degrees of freedom, and the orbital order for most of these phases has been theoretically proposed by Maezono *et al.*,[13] Khomskii,[22] van den Brink et al.,[35] and by Solovyev and Terakura.[36]

It is worth mentioning that there are some noticeable exceptions from this universal phase diagram: e.g., the Sm:Ca (Ref. 14) and the Pr:Ca (Refs. 14,34) compounds do not exhibit a typical CMR regime with a ferromagnetic and insulating ground state for $x < 0.5$. This fact probably results from geometrical constraints. In addition, peculiarities show up close to half filling: In the Nd:Sr and Pr:Sr compounds close to $x = 0.5$ charge-ordered antiferromagnetic phases were found.[30] Magnetically these systems form ferromagnetic zigzag chains that are coupled antiferromagnetically. This *CE*-type of magnetic structure results from charge and orbital order and has been explained theoretically in detail.[35,36] The FM zigzag chains with their concomitant charge order can easily be molten by the application of moderate magnetic fields.[37] In addition, van den Brink *et al.*[35] have shown that for doping $x < 0.5$ the *CE* structure is unstable against phase separation. This *CE*-type spin structure with a checkerboard-type CO is not observed in the La:Sr compound under investigation. In our high-quality samples, we find an AFM and metallic ground state with no signs of charge order. Hence we do not expect to find a *CE*-type magnetic structure. A metallic AFM spin *A*-type phase has been predicted by Maezono *et al.*,[13] which reveals an $(x^2\text{-}y^2)$ orbital structure. In this structure hopping along *c* is forbidden and the metallic conductivity is strictly two dimensional and indeed this type of behavior has been observed in $Nd_{0.45}Sr_{0.55}MnO_3$.[32] We believe that this type of spin and orbital structure may also be present in $La_{1-x}Sr_xMnO_3$ for $x \approx 0.6$. Measurements of the magnetic structure and of the anisotropy of the electronic transport still have to be performed. It remains a puzzle why in $Nd_{0.45}Sr_{0.55}MnO_3$, which reveals a metallic spin *A*-type phase, Kuwahara *et al.*[32] observed a significant anisotropy in the resistivity but not in the magnetic susceptibility. In contrast $La_{0.45}Sr_{0.55}MnO_3$ exhibits a pronounced anisotropy both in the FM and in the AFM states (cf. Fig. 6). It seems clear that the FM metallic state at elevated temperatures still is driven by double exchange, and perhaps the low-temperature metallic state indicates electronic phase separation where the FM metallic paths still percolate. The occurrence of a FM metal followed by an AFM metallic state for concentrations close to $x = 0.6$ still is a puzzle and further experimental work is needed to elucidate this strange phase.

ACKNOWLEDGMENTS

This work was supported by the Bundesministerium für Bildung und Forschung (BMBF) via Grant No. VDI/EKM, FKZ 13N6917, by the Deutsche Forschungsgemeinschaft via Grant No. SFB 484 (Augsburg), and by INTAS via Project No. 97-30850.

[1] R. von Helmolt, J. Wecker, B. Holzapfel, L. Schultz, and K. Samwer, Phys. Rev. Lett. **71**, 2331 (1993); K. Chahara, T. Ohono, M. Kasai, Y. Kanke, and Y. Kozono, Appl. Phys. Lett. **62**, 780 (1993).
[2] E. Dagotto, T. Hotta, and A. Moreo, Phys. Rep. **344**, 1 (2001).
[3] P.G. de Gennes, Phys. Rev. **118**, 141 (1960).
[4] A.J. Millis, B.I. Shraiman, and R. Mueller, Phys. Rev. Lett. **77**, 175 (1996).
[5] Y. Endoh, K. Hirota, S. Ishihara, S. Okamoto, Y. Murakami, A. Nishizawa, T. Fukuda, H. Kimura, H. Nojiri, K. Kaneko, and S. Maekawa, Phys. Rev. Lett. **82**, 4328 (1999).
[6] M. Paraskevopoulos, F. Mayr, J. Hemberger, A. Loidl, R. Heichele, D. Maurer, V. Mueller, A.A. Mukhin, and A.M. Balbashov, J. Phys.: Condens. Matter **12**, 3993 (2000); M. Paraskevopoulos, F. Mayr, Ch. Hartinger, A. Pimenov, J. Hemberger, P. Lunkenheimer, A. Loidl, A.A. Mukhin, V.Yu. Ivanov, and A.M. Balbashov, J. Magn. Magn. Mater. **211**, 118 (2000).
[7] T. Niemoeller, M. von Zimmermann, S. Uhlenbruck, O. Friedt, B. Büchner, T. Frello, N.H. Andersen, P. Berthet, L. Pinsard, A.M. de Leon-Guevara, A. Revcolevschi, and J.R. Schneider, Eur. Phys. J. B **8**, 5 (1999).
[8] J. B. Goodenough and J. M. Longo, in *Magnetic and Other Properties of Oxides and Related Compounds*, edited by K.-H. Hellwege and A. M. Hellwege, Landolt-Börnstein, New Series, Group III, Vol. 4 (Springer-Verlag, Berlin, 1970), p. 126.
[9] A. Urushibara, Y. Moritomo, T. Arima, A. Asamitsu, G. Kido, and Y. Tokura, Phys. Rev. B **51**, 14 103 (1995).
[10] Y. Yamada, O. Hino, S. Nohdo, R. Kanao, T. Inami, and S. Katano, Phys. Rev. Lett. **77**, 904 (1996).
[11] H. Kawano, R. Kajimoto, M. Kubota, and H. Yoshizawa, Phys. Rev. B **53**, R14 709 (1996).
[12] J.-S. Zhou, J.B. Goodenough, A. Asamitsu, and Y. Tokura, Phys. Rev. Lett. **79**, 3234 (1997).
[13] R. Maezono, S. Ishihara, and N. Nagaosa, Phys. Rev. B **57**, 13 993 (1998); **58**, 11 583 (1998), and references therein.
[14] C. Martin, A. Maignan, M. Hervieu, and B. Raveau, Phys. Rev. B **60**, 12 191 (1999).
[15] T. Akimoto, Y. Maruyama, Y. Moritomo, A. Nakamura, K. Hirota, K. Ohoyama, and M. Ohashi, Phys. Rev. B **57**, R5594 (1998).
[16] Y. Moritomo, T. Akimoto, A. Nakamura, K. Ohoyama, and M. Ohashi, Phys. Rev. B **58**, 5544 (1998).
[17] H. Fujishiro, T. Fukase, and M. Ikebe, J. Phys. Soc. Jpn. **67**, 2582 (1998).
[18] S.I. Patil, S.M. Bhagat, Q.Q. Shu, S.E. Lofland, S.B. Ogale, V.N. Smolyaninova, X. Zhang, B.S. Palmer, R.S. Decca, F.A. Brown, H.D. Drew, R.L. Green, I.O. Troyanchuk, and W.H. McCarroll, Phys. Rev. B **62**, 9548 (2000).
[19] A. Arrot and J.E. Noakes, Phys. Rev. Lett. **19**, 786 (1967).
[20] P.G. Radaelli, D.E. Cox, L. Capogna, S.-W. Cheong, and M. Marezio, Phys. Rev. B **59**, 14 440 (1999).
[21] S. Mori, C.H. Chen, and S.-W. Cheong, Nature (London) **392**, 479 (1998); Phys. Rev. Lett. **81**, 3972 (1998).
[22] D.I. Khomskii, cond-mat/0104517 (unpublished); D.I. Khomskii and K.I. Kugel, Europhys. Lett. **55**, 208 (2001).
[23] K. Held and D. Vollhardt, Phys. Rev. Lett. **84**, 5168 (2000); K. Held and D. Vollhardt, Eur. Phys. J. B **5**, 473 (1998).
[24] J. van den Brink and D. Khomskii, Phys. Rev. Lett. **82**, 1016 (1999).
[25] For an overview of the different types of spin structures in perovskites the reader is referred to: J. B. Goodenough, *Magnetism and the Chemical Bond* (Wiley, New York, 1963), p. 94.
[26] A.M. Balbashov, S.G. Karabashev, Ya.M. Mukovskiy, and S.A. Zverkov, J. Cryst. Growth **167**, 365 (1996).
[27] A. Krimmel, J. Hemberger, A. A. Mukhin, A. Balbashov, and A. Loidl (unpublished).
[28] P.G. Radaelli, D.E. Cox, M. Marezio, and S.-W. Cheong, Phys. Rev. B **55**, 3015 (1997).
[29] M.R. Lees, J. Barratt, G. Balakrishnan, D.M. Paul, and C. Ritter, Phys. Rev. B **58**, 8694 (1998).
[30] H. Kawano, R. Kajimoto, H. Yoshizawa, Y. Tomioka, H. Kuwahara, and Y. Tokura, Phys. Rev. Lett. **78**, 4253 (1997).
[31] M. Hervieu, G. Van Tendeloo, V. Caignaert, A. Maignan, and B. Raveau, Phys. Rev. B **53**, 14 274 (1996).
[32] H. Kuwahara, T. Okuda, Y. Tomioka, A. Asamitsu, and Y. Tokura, Phys. Rev. Lett. **82**, 4316 (1999).
[33] P. Schiffer, A.P. Ramirez, W. Bao, and S.-W. Cheong, Phys. Rev. Lett. **75**, 3336 (1995); A.P. Ramirez, P. Schiffer, S.-W. Cheong, C.H. Chen, W. Bao, T.T.M. Palstra, P.L. Gammel, D.J. Bishop, and B. Zegarski, *ibid.* **76**, 3188 (1996).
[34] Y. Tomioka, A. Asamitsu, H. Kuwahara, Y. Moritomo, and Y. Tokura, Phys. Rev. B **53**, R1689 (1996).
[35] J. van den Brink, G. Khaliullin, and D. Khomskii, Phys. Rev. Lett. **83**, 5118 (1999).
[36] I.V. Solovyev and K. Terakura, Phys. Rev. Lett. **83**, 2825 (1999).
[37] H. Kuwahara, Y. Tomioka, A. Asamitsu, Y. Morimoto, and Y. Tokura, Science **270**, 961 (1995).